Progress in Natural Science: Materials International xxx (xxxx) xxx–xxx

HOSTED BY

ELSEVIER

Contents lists available at ScienceDirect

Progress in Natural Science: Materials International

journal homepage: www.elsevier.com/locate/pnsmi

Original Research

Structural and dielectric study of nano-crystalline single phase $Sn_{1-x}Ni_xS$ (x_{Ni}=0–10%) showing room temperature ferromagnetism☆

B. Parveen[a], M. Hassan[a,*], S. Atiq[b], S. Riaz[b], S. Naseem[b], M. Asif Toseef[c]

[a] Materials Growth and Simulation Laboratory, Department of Physics, University of the Punjab, Lahore 54590, Pakistan
[b] Centre of Excellence in Solid State Physics, University of the Punjab, Lahore 54590, Pakistan
[c] Department of Physics, Govt. Islamia College, Narowal, Pakistan

ARTICLE INFO

Keywords:
Diluted magnetic semiconductors
Room temperature ferromagnetism
Near edge x-ray absorption fine structure spectroscopy
Dielectric properties
Co-precipitation method

ABSTRACT

SnS is a promising IV-VI semiconductor, which is very less explored for diluted magnetic semiconducting and dielectric applications. In this study, the Ni doping (x_{Ni}=0–10 mol%) effects on SnS host lattice were investigated. A simple and low cost co-precipitation technique was employed to grow Ni doped SnS powders. The X-ray diffraction confirmed single phase orthorhombic structure with a nano-crystalline nature that was further verified through the surface structure observed by scanning electron microscopy. Near edge x-ray absorption fine structure spectroscopy revealed a shift in the Ni absorption edge towards higher energy, depicting the formation of Ni^{+3} oxidation state. The impedance measurements, in the frequency range 1 kHz to 20 MHz, depict that owing to the excellent sensitivity to the electromagnetic radiations at the low energy, the Ni doped SnS finds potential applications in various energy related devices. Vibrating sample magnetometer measurements have elucidated room temperature ferromagnetism, which depicts potential memory device applications.

1. Introduction

In recent years, novel and advance materials are being explored to achieve highly efficient data storage and spintronic devices. The diluted magnetic semiconductors (DMS), which simultaneously exhibit semiconducting and ferromagnetic behaviors [1], generally have holes in the valence band, which are responsible to induce ferromagnetic interactions between the localized spins of the magnetic impurity elements. The DMS are formed by substituting small fraction of the cations of the host nonmagnetic semiconductor lattice with magnetic impurities [2]. Owing to the carrier-mediated ferromagnetism, DMSs can be employed for information processing and data storage functionalities [3]. Transition metals can be employed as dopant for II-VI, IV-VI and III-V binary compound semiconductors to control both charge and spin of electrons to realize spintronic devices capable to modulate magnetic properties through external electric fields [4]. IV-VI DMS also show carrier concentration alterations by controlling native defects, which can also be employed to manipulate ferromagnetism [5]. Among many IV-VI semiconductors, Tin mono-sulphide (SnS) is the most promising material that stabilizes in the orthorhombic structure [6]. The SnS exhibit layered structure, in which subsequent layers are coupled through weak van der walls forces [7]. In addition to SnS, other phases like SnS_2 and SnS_3 currently have also gained many interests because their constituent elements, Sn and S, are non-toxic, inexpensive and are abundant [8]. The band gap of SnS, can be adjusted to the ideal value of 1.5 eV that is most suitable for solar cell applications [9], where a high absorption coefficient ($> 10^4$ cm^{-1}) [10], high conversion efficiency ~25% is possible to achieve. Moreover, it can also exhibit both p-type and n-type conduction [11]. Un-doped SnS always show p-type character, while, doping with suitable dopant may leads to n-type conduction [12,13]. A variety of reports exist about SnS doping to improve the photovoltaic and optoelectronic properties. For example, Ag doped SnS thin films [14] have been prepared to study the doping induced changes in the structural, dielectric and optical properties and reported that doping decreases the resistivity up to 10^{-3} Ω cm. Ninan et al. [15] have prepared Cu doped SnS thin films by spray pyrolysis and have observed that doping improves the optoelectronic properties of SnS. In another report about Fe doped SnS thin films [16], which are fabricated by chemical bath deposition, and it has been shown that current density is controllable by Fe doping. Similarly, Saminathan [17], have characterized Co and Fe doped SnS nanoparticles, synthesized by precipitation route, and explored that doping affects structural and optical properties, which make this material suitable for optoelectronic devices.

Peer review under responsibility of Chinese Materials Research Society.
* Corresponding author.
E-mail address: mahmood.physics@pu.edu.pk (M. Hassan).

http://dx.doi.org/10.1016/j.pnsc.2017.04.007
Received 18 November 2016; Received in revised form 15 March 2017; Accepted 10 April 2017

All reports about SnS have only considered photovoltaic and optoelectronic applications. The diluted magnetic semiconducting characteristics could be generated in SnS by doping with transition elements that could be attractive for fundamental research and technological applications. Up to the best of our knowledge, no experimental report on Ni doped SnS exist in the literature, which has motivated us for the present study to explore DMS applications of the Ni doped SnS. In this study, we present the structural, surface morphological, dielectric and ferromagnetic characteristics of $Sn_{1-x}Ni_xS$ (x_{Ni} =0–10%), to show that the synthesized DMS respond to incident frequency and exhibit ferromagnetic behaviors, suggesting dielectric and data storage device applications.

2. Experimental details

Co-precipitation was employed to prepare un-doped and Ni doped SnS by using analytical grade $SnCl_2$, Na_2S and $NiCl_2$ precursors. The un-doped SnS was prepared by taking stoichiometric molar amounts of $SnCl_2$ and Na_2S separately in 50 ml of deionized water. The solutions were stirred at room temperature (RT) for 15 min, by using magnetic stirrer on a hot plate. Both solutions were mixed drop-wise and stirred until a dark brown colored thick precipitates appear indicating SnS nanoparticle formation. After filtration and washing, the precipitates were dried at 50 °C in an electric oven. Similar procedure was repeated to prepare Ni doped SnS, with x_{Ni}=2–10 mol%. During $SnCl_2$ solution preparation, the required quantity of $NiCl_2$ was added to achieve requisite Ni molar composition. The structural investigations were done with Rigaku X-ray diffractometer (XRD), R-AXIS IV^{++} with a Mo Kα radiations and the diffraction pattern was recorded on 2D image plate. Later, the wavelength was changed to Cu Kα for the sake of comparison with the literature. The 2D image was converted to 1D graph using GSAS II program. The surface structures were elucidated by using scanning electron microscopy (SEM) (EF-SEM NOVA NanoSEM200, EFI). Near edge x-ray absorption fine structure (NEXAFS) spectra around Ni L-edge were observed at 10D KIST beamline, by employing bending magnet at Pohang Light source (PLS-II). The dielectric characterization was done by employing 6500B impedance analyzer (LCR meter). The ferromagnetic investigations were performed by employing Lakeshore 7404 vibrating sample magnetometer (VSM).

3. Results and discussions

3.1. Structural characterization

The x-ray diffraction (XRD) was employed to observe the crystallographic structure of the grown un-doped and Ni doped SnS. The measured line scans are presented in Fig. 1. All the samples exhibited orthorhombic crystal structure due to exact match with JCPDS card no. 00–001–0984. The polycrystalline nature of the fabricated samples was evident from the various crystallographic planes contributing to the diffraction process. Moreover, XRD patterns of Ni doped and un-doped SnS did not have considerable differences that evidence the single phase formation. Moreover, no peak belongs to any other Sn based phases like SnS_2 or any secondary phase belonging to Ni impurity. It can also be observed that all the samples preferably grow along (013) direction. Degree of crystallinity has been observed to increase with Ni doping. The orthorhombic lattice constants for un-doped and Ni doped SnS were computed by employing expression as follow [18].

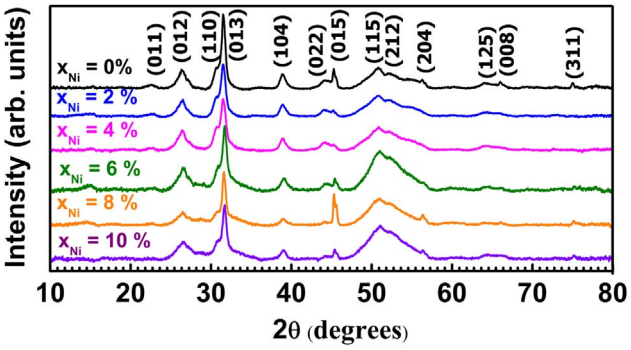

Fig. 1. XRD line scans for SnS with x_{Ni}=0–10%.

$$\frac{1}{d^2} = \frac{h^2}{a^2} + \frac{k^2}{b^2} + \frac{l^2}{c^2} \quad (1)$$

where (h k l) represents miller indices and a, b, c, are the lattice constants. The calculated lattice constants are plotted against Ni content, as presented in Fig. 2(a). The lattice constants were observed to show an overall decreasing tendency with Ni content, which might be due to the incorporation of Ni^{+2} ion having a smaller ionic radius (0.69 Å) as compared to the ionic radius of Sn^{+2} (0.93 Å) in the SnS host lattice, which induces lattice shrinkage, and as a result lattice constants decrease. The corresponding unit cell volume as depicted in Table 1 also decreases from 192 Å to 191 Å in SnS with x_{Ni}=0–10%, respectively. The calculated values of lattice constants for un-doped SnS, as presented in Table 1, are in good agreement with the JCPDS card no. 00-001-0984 as well as with the literature (a=3.99 Å, b=4.34 Å, c=11.20 Å) [18]. The diffraction peak broadening is very important parameter to calculate crystallite size and strain. Debye-Scherer formula [19] was used to evaluate crystallite size from XRD peaks as given below

$$D = \frac{k\lambda}{\beta_{hkl}\,\mathrm{Cos}\,\theta} \quad (2)$$

where k represents the shape factor which is equal to 0.9, β_{hkl} is the full-width at half-maximum taken in radians and λ is x-ray wavelength. The calculated crystallite size for un-doped SnS is 13.7 nm, as presented in Fig. 2(b). Increasing Ni content to 2% caused decrease in the crystallite size to 10 nm. While on further increasing the Ni content from 4% to 10%, the crystallite size continuously increased and approached to 20.1 nm. Fig. 2(b) shows an overall increasing tendency of crystallite size with Ni content. The crystallite size is in close agreement to already reported values, for example, Jakhar et al. reported that SnS thin films have crystallite size in the range 11–25 nm [20]. The increase in crystallite size can be correlated with the variations in the lattice parameters. Because the decreasing lattice constant shows that lattice shrinks and more ions can be accommodate during growth and therefore, the grain growth occurs which enhances the net crystallite size. The residual strain within the samples arising due to lattice defects was computed by employing Stokes-Wilson equation [21,22], as given below.

$$\varepsilon = \frac{\beta_{hkl}}{4tan\theta} \quad (3)$$

The strain is 0.0122 for un-doped SnS. The increase in Ni impurity content to 2–6% decreased the strain to 0.008 and remains in this range until Ni content was further increased from 6% to 10%. It can be observed that there was an overall decreasing trend of strain with increasing Ni content, which is closely related to the increase in crystallite size that only appears if the strain relaxation occurs. Hence, the increase in crystallite size appears with the decreasing strain which is due to the decrease in lattice defects. Moreover, the calculated crystallite size has a nanometer range that shows the nano-crystalline nature of the grown samples and depicts potential applications of the prepared DMSs in memory devices with reduced dimensions. Furthermore, the crystallite size 'D' and strain 'ε' were also calculated by employing Williamson-Hall plot method by using the following equation [23].